16B-04 X-BAND MARINE RADAR DETECTION OF EJECTED LAPILLI AND VOLCANIC BLOCKS

M. Maki[1*], Y. Fujiyoshi[2], H. Tokushima[3], and M. Iguchi[4]
[1]Research and Education Center for Natural Hazards, Kagoshima University
[2] Emeritus Prof., Hokkaido University
[3]Field Researchers Corporation
[4]Disaster Prevention Research Institute, Kyoto University

1. INTRODUCTION

Pyroclastic materials (or tephra) are grouped into three categories, based on size: volcanic ash (≦2 mm, lapilli (2 mm- 64 mm), and volcanic blocks (≧64 mm). Following volcanic eruptions, volcanic ash particles suspended in the atmosphere can cause aviation accidents and force airports to shut down, and volcanic ash deposited on the ground can cause traffic disturbances. Larger tephra, such as lapilli and volcanic blocks (hereinafter referred to as 'large tephra'), which are ejected from volcanic vents just after explosive volcanic eruptions, can directly cause injury to humans and damage to property. For example, in the eruption that occurred at Mt. Ontake, Japan on September 27, 2014, sixty-three hikers were killed or went missing as a direct result of the large tephra ejected during the eruption (Tsunematsu et al., 2016; Yamaoka et al., 2016). In the area surrounding the active volcano Sakurajima, pupils are required to wear helmets on their way to and from school. In anticipation of future large eruptions, the Kagoshima City government has provided helmets and evacuation manuals to all residents in Sakurajima. Shelters are also set up alongside the city's main streets for emergency use during eruptions. To make the above-mentioned countermeasures more effective, monitoring and the prompt communication of information are required.

The methods available for monitoring large tephra have basically been limited to camera and naked eye observations, which are ineffective in cloudy or rainy conditions. Although recent studies demonstrate the usefulness of weather radars for monitoring volcanic ash and estimating quantitative ash falls, their use for large tephra monitoring has not been successful. One of main reasons for the lack of success is that most of the weather radars in those studies used pencil beams transmitted from a parabolic antenna, rotating at 2 to 6 rpm; the possibility of a pencil beam illuminating a moving large tephra is extremely low. The present study tries to solve this problem by utilizing a marine radar, which utilizes a fan beam and has fast scanning capabilities.

From the volcanology perspective, information on tephra fall from vents is one of the key factors in eruption dynamics (e.g., Bursik et al., 1992; Sparks et al., 1992) and magma dynamics (e.g., Kaminski and Jaupart, 1998). Several studies, using high speed cameras and meteorological instruments, have been performed based on geological methods such as size distribution measurements of tephra deposits (Kozono et al. 2019). Although the present study tries to estimate trajectories of tephra ejected from a vent, the main purpose is to assess the potential of marine radar for monitoring tephra and for the mitigation of volcanic hazards.

* Corresponding author address: Masayuki Maki, Kagoshima Univ., Research and Education Center for natural Hazards, Korimoto 1-21-40, Kagoshima, 890-0065, Japan; e-mail: maki@gm.kagoshima-u.ac.jp

2. OBSERVATIONS

2.1 Marine radar

Table 1 shows the main specification of the marine radar used in the present study. The marine radar is an X-band non-Doppler radar, which has a slot antenna with a vertical beam width of 22° and a horizontal beam width of 1.2°, a minimum range resolution of 8 m, and a PPI scanning speed of 48 rpm. We manually changed the rotational axis of the slot antenna, from vertical to horizontal, to achieve an elevation angle resolution of 1.2°. The resulting image data files, recorded at 1.25-second intervals, make it possible to detect both an eruption and the large tephra being ejected above the vent.

Table 1 Main specification of marine radar.

Antenna	Length	197 cm
	Beam width	H: 1.2°, V: 22°
	Scan speed	24, 48 24 rpm
	Polarization	H
Transmitter	Peak power	25kW
	Pulse width	0.08, 0.2, 0.3, 0.6, 1.2 μs
	PRF	5, 15 MHz
	Range resolution	12, 30, 45, 90, 180 m
Monitor	Size	19 inch colour LCD
	Resolution	1280×1024 pixcel
	Range accuracy	8 m

The marine radar was installed at the Kyoto University Kurokami observatory (N 31° 35' 00.5", E130° 42' 06.2", 68 m), indicated by the letter 'B' in Fig. 1. The distance from the radar to the Minamidake vent (N 31° 34' 47.0", E130° 39′, 39.30", 1040 m) is approximately 4 km.

2.2 Free fall experiments

Before utilizing the marina radar to carry out observations of actual volcanic eruptions, we

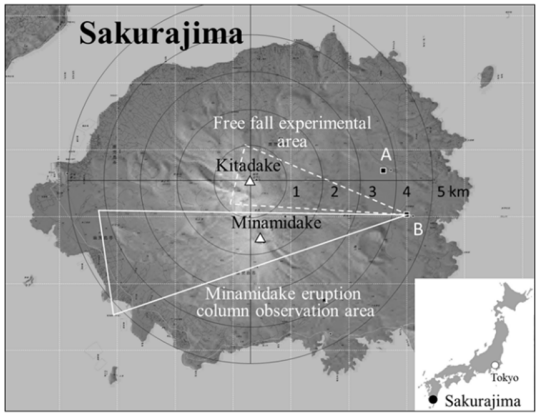

Fig. 1 Map showing radar observation area for the free fall experiments and Minamidake volcanic eruption column observations. A: Ku-band Doppler radar (Maki et al., 2019) site. B: X-band marine radar site.

examined its capabilities by performing a simulation

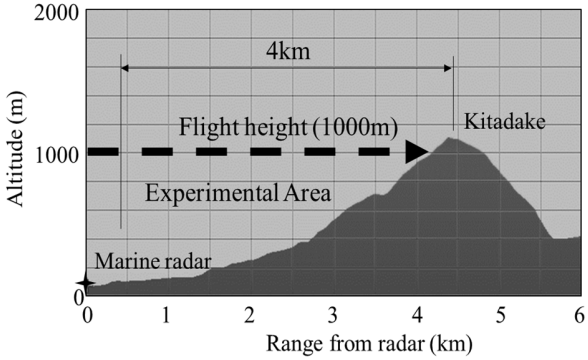

Fig. 2 Vertical cross section along the radar beam azimuth direction, which is determined from the environmental wind field. Free fall experimental area.

where artificial particles were dropped from a small airplane (Cessna 172P), flying at an altitude of approximately 1000 m at a speed of 185 km h^{-1}. Figure 2 shows the vertical cross section of the free fall experimental area. The direction of the vertical cross section corresponds to the radar beam azimuth direction which was determined considering the vertical wind direction and the topographical features of Sakurajima.

Three different kinds of artificial particles were examined: water droplets (hereinafter Sample 1), 'tamakonnyaku' particles (hereinafter Sample 2) which consist mainly of water, with some glucomannan, and 'fu' particles (hereafter Sample 3) which are sponge-like processed foods made from wheat gluten. The size of each artificial particle was around 3 cm in diameter, except for the water droplets. A 5- liter bucketful of the artificial particles and water droplets was ejected from the airplane into the air. The drops were done in such a way that the released particles fell through the radar beam, which is shown as a broken white circular sector in Fig, 1. The dropping of particles was done twice for each type of sample.

2.3 Observations of volcanic eruptions

The target of the radar observations of actual volcanic eruptions is pyroclastic material, which are divide into three main categories according to size: volcanic blocks (> 64 mm), lapilli (64 mm - 2 mm), and volcanic ash (< 2 mm). In order to detect actual pyroclastic materials, the X-band marine radar antenna direction was fixed in the azimuth direction, looking at the Minamidake vent (Fig. 1), and observations with RHI antenna scanning were carried out. The geometrical radar beam is shown as a solid white circular sector in Fig. 2. The observation period was approximately from April 11 to May 31 (a total of 51 days). The collected data was for a total of 57 eruptions, of which 49 eruptions were explosive.

3. RESULTS

3.1 Free fall experiments

3.1.1 Detection of water droplets (Sample 1)

The airplane used in the simulations is itself a good reflector because it is made of metals. The marine radar could detect the airplane while it was flying in the radar illuminated area. From a series of observed RHI images, it was possible to estimate the height at which the airplane was flying. Water droplets are also good reflectors of electric waves and we expected that the marine radar would be able to detect them. However, the radar detected no echo from the water droplets. This is probably due to the water turning into mist sized

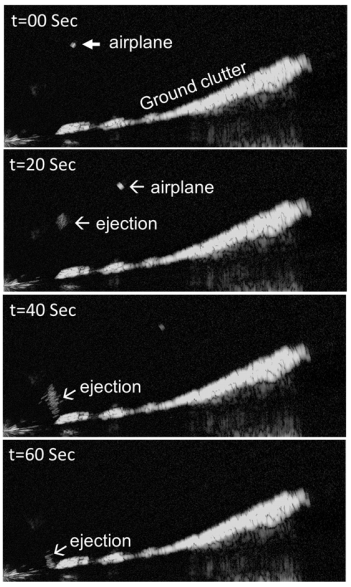

Fig. 3 A series of RHI images showing the descending echoes of ejections (Sample 2).

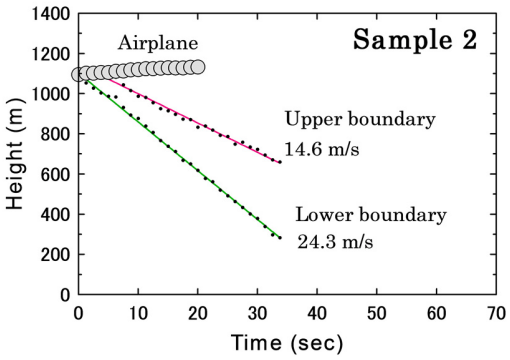

Fig. 4 Trajectories of upper and lower boundaries of Sample 2 echoes.

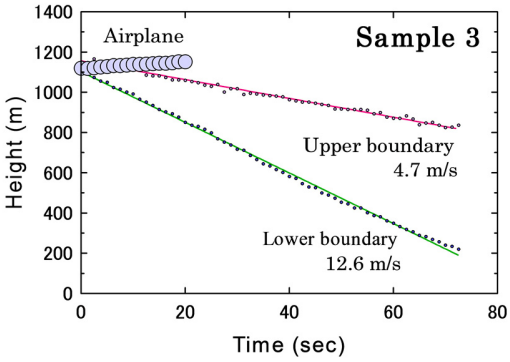

Fig. 6 Same as Fig. 4 except for Sample 3 echoes.

particles immediately following its ejection from the airplane.

3.1.2 Detection of 'tamakonnyaku' (Sample 2)

The marine radar successfully detected falling 'Sample 2' particles, as shown by a time series of RHI images of radar data (Fig.3). One can recognize as the airplane, which was traveling from left to right at around 1000 m above sea level. It can also be seen in Fig. 3

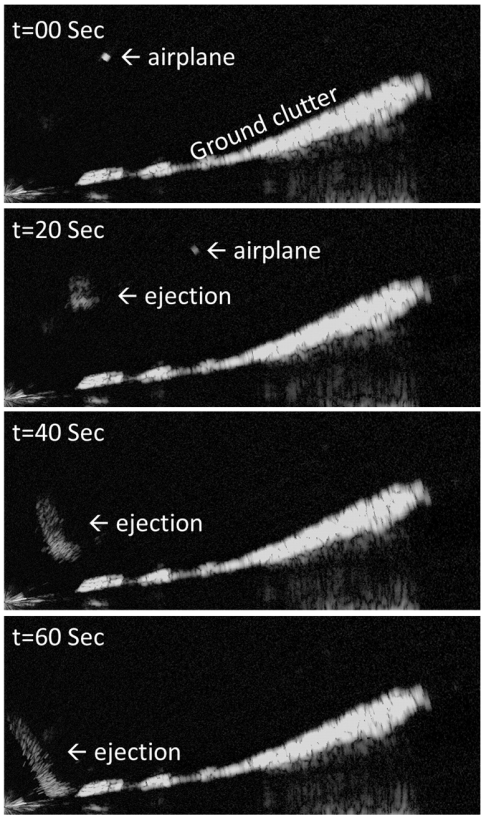

Fig. 5 Same as Fig. 3 except for the echoes of ejections (Sample 3).

that the echoes of Sample 2 particles are descending from the airplane to the ground. It should be noticed that the echoes are stretching vertically during their descent. By identifying sample 1 echoes on a series of radar images, which has a spatial resolution of 4.34 m and temporal resolution of 1.25 s, we can analyze their trajectories and estimate their terminal velocities. Figure 4 shows the result of this analysis. The estimated terminal velocities at the upper boundary and the lower boundary of echoes are 14.6 m s^{-1} and 24.3 m s^{-1}, respectively. This speed difference is considered to be caused by the group effect of falling particles, i.e., decreases in the drag force (e.g., Harada et al., 1964).

3.1.3 Detection of wet 'fu' (Sample 3)

The marine radar also succeeded in detecting released 'Sample 3' particles all the way to the ground (Fig. 5). However, the echo patterns of Sample 3 particles are more vertically stretched compared to 'Sample 2' particles, which is due to 'Sample 3' particles being easily segmentalized by air resistance. The segmentation of particles causes a decrease in their terminal velocities in addition to vertically stretching their echoes. The terminal velocities at the upper and lower boundaries of echoes is estimated as 4.7 m s^{-1} and 12.6 m s^{-1}, respectively (Fig. 6).

3.2 Tephra from Minamidake eruptions

3.2.1 Statistics of tephra detection with marine radar

According to the Japan Meteorological Agency (JMA), a total of 57 eruptions occurred at the Sakurajima Minamidake vent during our radar observation periods. The marine radar could detect large tephra in 40 of those eruptions (70 % of all eruptions), while JMA, based on visual observations, reported the ejected the large tephra in 35 of the same eruptions. It therefore follows that the marine radar detection of large tephra is consistent with JMA visual observations. As far as we know, this study presents the first successful detection of a volcanic eruption and the simultaneous detection of falling large tephra. The radar also revealed the fine structure of an ascending

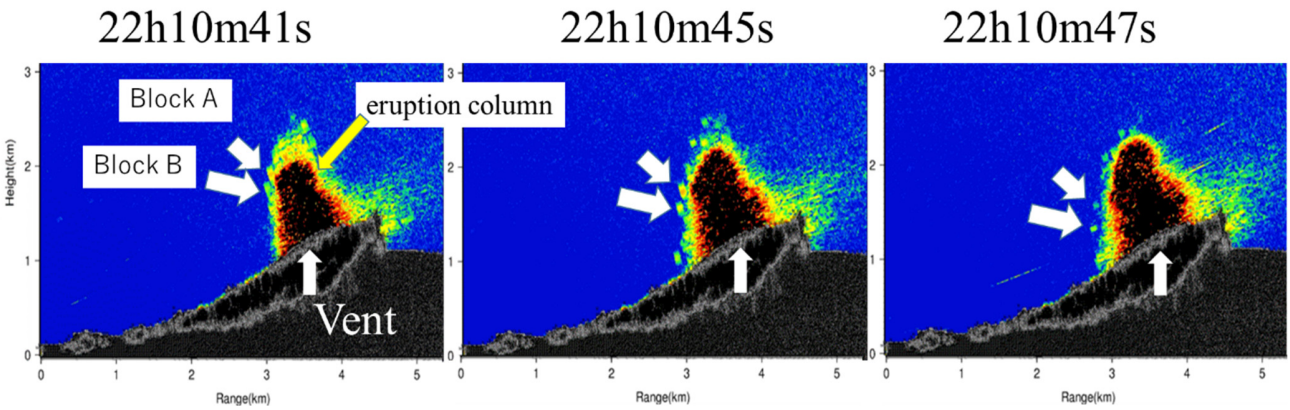

Fig. 6 Range-height radar images of an eruption column and volcanic blocks from 22h10m41s to 22h10m47s on 4 May, 2018.

eruption column, which implied another advantage of marine radar for the monitoring of volcanic eruption columns.

3.2.2 Ballistic trajectories of volcanic blocks

Several models are available for the calculation of the ballistic trajectories of volcanic blocks (e.g., Wilson 1972; Fagents and Wilson 1993; Bower and Woods 1996; Tsunematsu et al., 2014; 2019). The main forces acting on the volcanic blocks are gravity and air drag force. The value of the air drag coefficient (Cd) assumed by most of the available models ranges from 0.65 to 1.21, as reported by Alatorre-Ibargu¨engoitia and Delgado-Granados (2006). However, it is quite difficult to detect the ballistic trajectories of volcanic blocks while working in the field and to observationally determine the value of Cd.

Figure 6 shows radar images of an eruption column and volcanic blocks from 22h10m41s to 22h10m47s on 4 May, 2018. The horizontal speeds of the two blocks were almost constant, that is, UA= 38 and UB= 41 m s^{-1}, respectively. Volcanic block height is approximated well by the following parabolic equation:

$$H(t) = \alpha \cdot t^2 + \beta \cdot t + \gamma$$

The values of α for block-A and block-B are -4.93 and -4.79, respectively, and not far from -1/2 g=-4.90 m s^{-2}. We also analyzed radar images obtained from 10h14m30s to 10h30m38s on 17 May, 2018 (block-C).

We can estimate the initial velocities (V0) and ejection angles (θ) of three blocks if we interpolate the trajectories to the place of the vent where blocks are ejected; that is, (V0, θ) = (121 m s^{-1}, 70.9°) (block-A), (141 m s^{-1}, 70.5°) (block-B) and (108 m s^{-1}, 69.4°) (block-C) respectively. Figure 7 shows the ballistic trajectories of three blocks based on the radar observation. We also calculate ballistic trajectories of three blocks using the program “Eject !” provided by U. S. geological Survey (Mastin, 2001). We assume the block to be a 1 m diameter sphere with a density of 2500 kg/m3, and use the default values for parameters except for air drag coefficient (Cd). As shown in Fig. 7, the calculated ballistic trajectories represent the ones

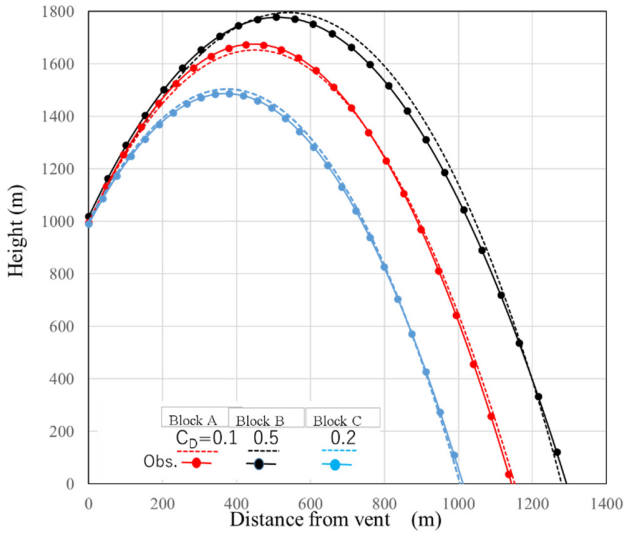

Fig. 7 Observed and simulated ballistic trajectories of three volcanic blocks

observed when the air drag coefficients (Cd) are 0.1 (block-A), 0.5 (block-B) and 0.2 (block-C).

5. SUMMARY

Up to the present, some researchers have studied volcanic activity using high speed movies/videos (Chouet et al. 1974; Taddeucci et al. 2012), still camera images (Iguchi et al. 1983), infrared film cameras (Ripepe et al. 1993), a Forward Looking Infrared Radiometer (FLIR) camera (Patrick et al. 2007), and an FM-CW Doppler K-band radar (Hort and Syfired 1998; Hort et al. 2003). In the present work, we estimated the ballistic trajectories of volcanic blocks by utilizing a vertically scanning X-band marine-radar. As far as the authors are aware, the present paper reports the first successful detection by radar of volcanic blocks.

Acknowledgements. This work was partially supported by Council for Science, Technology and Innovation(CSTI), Cross-ministerial Strategic Innovation Promotion Program 2 (SIP2), “National Resilience” (Funding agency: NIED) and partially supported by the collaborative research program (30G-01) of the Disaster Prevention Research Institute of Kyoto University.

References

Alatorre‐Ibargüengoitia, Miguel, A., and Hugo Delgado‐Granados, 2006: Experimental determination of drag coefficient for volcanic materials: calibration and application of a model to Popocatépetl volcano (Mexico) ballistic projectiles. *Geophys. Res. Let*., **33**.11.

Bower, S. M. and A. W. Woods, 1996: On the dispersal of clasts from volcanic craters during small explosive eruptions. *J. Volcanol. Geotherm. Res.*, **73**, 19-32.

Bursik M. I., R. S. J. Sparks, J. S. Gilbert and S. N. Carey, 1992: Sedimentation of tephra by volcanic plumes: I. Theory and its comparison with a study of the Fogo A plinian deposit, Sao Miguel (Azores). *Bull. Volcanol.* **54**, 329–344. doi: 10.1007/BF00301486

Chouet, B., N. Hamisevicz, and T. R. McGetchin, 1974: Photoballistics of volcanic jet activity at Stromboli, Italy. *J. Geophys. Res.*, **79**, 4961–4976.

Fagents, S. A. and L. Wilson, 1993: Explosive volcanic eruptions; VII, The ranges of pyroclasts ejected in transient volcanic explosions. *Geophys. J. Int.*, **113**, 359-370.

Harada, S., H. Narui, K. Shimada, T. Fukushima, 1964: Terminal Velocity of Particle Group: Fundamental Research on Pneumatic Conveying. *Trans. Japan Soc. Mech. Eng*., **30**, 231-235. (Japanese with English abstract), https://doi.org/10.1299/kikai1938.30.231

Hort, M. and R. Seyfried, 1998: Volcanic eruption velocities measured with a micro radar. *Geophys. Res. Lett.*, **25**,113–116.

Hort, M., R. Seyfried and M. Vöge, 2003: Radar Doppler velocimetry of volcanic eruptions: theoretical considerations and quantitative documentation of changes in eruptive behaviour at Stromboli volcano, Italy. *Geophys. J. Int.*, **154**, 515-532.

Iguchi, M., K. Ishihara and K. Kamo, 1983: On ejection velocity and pressure of volcanic eruption reduced from photo-trajectory of volcanic bombs. *Ann. Disast. Prev. Res.* Inst., Kyoto Univ., B-1, **36**, 9-21.

Kaminski E., and C. Jaupart, 1998: The size distribution of pyroclasts and the fragmentation sequence in explosive volcanic eruptions. *J. Geophys. Res.*, **103**(B12), 29759–29779. doi: 10.1029/98JB02795

Kozono, T., M. Iguchi, T. Miwa, M. Maki, T. Maesaka, D.Miki 2019: Characteristics of tephra fall from eruptions at Sakurajima volcano, revealed by optical disdrometer measurements. *Bull. Volcanol.*, **81**:41. DOI: 10.1007/s00445-019-1300-2

Maki, M., S. Takahashi, S. Okada, K. Imai, H. Yamaguchi, 2019: Ku-band high-speed scanning Doppler radar for volcanic eruption monitoring. *J. Disast. Res.*, 14, 630-640. https://doi.org/10.20965/jdr.2019.p0630

Mastin, L. G., 2001: A simple calculator of ballistic trajectories for blocks ejected during volcanic eruptions. *U.S. Geological Survey Open-File Report* 01-45, 16pp, https://pubs.usgs.gov/of/2001/0045/

Patrick, M. R., A. J. L. Harris, M. Ripepe, J. Dehn and D. A. Rothery, 2007: Strombolian explosive styles and source conditions: insights from thermal (FLIR) video. *Bull. Volcanol.*, **69**, 769-784.

Ripepe, M., M. Rossi and G. Saccorotti, 1993: Image processing of explosive activity at Stromboli. *J. Volcanol. Geotherm. Res.*, **54**, 335–351.

Sparks R.S.J., M.I. Bursik, G.J. Ablay, R.M.E. Thomas, S.N. Carey, 1992: Sedimentation of tephra by volcanic plumes. Part 2: controls on thickness and grain-size variations of tephra fall deposits. *Bull Volcanol* **54**, 685–695. doi: 10.1007/BF00430779

Taddeucci, J., P. Scarlato, A. Capponi, E. Del Bello, C. Cimarelli, D. M. Palladino and U. Kueppers, 2012: High‐speed imaging of strombolian explosions: The ejection velocity of pyroclasts. *Geophys. Res. Lett.*, **39**. doi:10.1029/2011GL050404

Tsunematsu, K., B. Chopard, J. L. Falcone and C. Bonadonna, 2014: A numerical model of ballistic transport with collisions in a volcanic setting. *Computers & geosciences*, **63**, 62-69. https://doi.org/10.1016/j.cageo.2013.10.016

Tsunematsu, K., Y. Ishimine, T. Kaneko, M. Yoshimoto, T. Fujii, and K. Yamaoka, 2016: Estimation of ballistic block landing energy during 2014 Mount Ontake eruption. *Earth, Planets and Space,* **68**: 88. https://doi 10.1186/s40623-016-0463-8

Tsunematsu, K., K. Ishii, and A. Yokoo, 2019: Transport of ballistic projectiles during the 2015 Aso Strombolian eruptions. Earth, *Planets and Space*, **71**:49.

Wilson, L., 1972: Explosive volcanic eruptions—II. The atmospheric trajectories of pyroclasts. Geophys. *J. R. Astr. Soc*. **30**, 381–392.

Yamaoka, K., N. Geshi, T. Hashimoto, S.E. Ingebritsen, and T. Oikawa, 2016: Special issue "The phreatic eruption of Mt. Ontake volcano in 2014". *Earth, Planets and Space*, **68**:175. https://doi.org/10.1186/s40623-016-0548-4